NUMERICAL SUBGRID UPSCALING OF TWO-PHASE FLOW IN POROUS MEDIA

Todd Arbogast

Abstract

We present an approach and numerical results for scaling up fine grid information to coarse scales in an approximation to a nonlinear parabolic system governing two-phase flow in porous media. The technique allows upscaling of the usual parameters porosity and relative and absolute permeabilities, and also the location of wells and capillary pressure. Some of these are critical nonlinear terms that need to be resolved on the fine scale, or serious errors will result. Upscaling is achieved by explicitly decomposing the differential system into a coarse-grid-scale operator coupled to a subgrid-scale operator, which we localize by imposing a closure assumption. We approximate the coarse-grid-scale operator with a mixed finite element method that has a second order accurate velocity coupled implicitly to the subgrid scale. The subgrid-scale operator is approximated locally by a first order accurate mixed method. A numerical Greens influence function technique allows us to solve these subgrid problems independently of the coarse-grid approximation. No explicit macroscopic coefficients nor pseudo-functions result. The method is easily seen to be optimally convergent in the case of a single linear parabolic equation.

KEYWORDS: upscaling, subgrid, numerical Greens functions, porous media

1 Introduction

In many physical problems, there are scales that are too fine to resolve on any reasonable computational mesh. The objective of upscaling or homogenization is to replace the governing equations by a simpler set of equations for which the solution can be resolved on a reasonable coarse-scale mesh and approximates the average behavior of the solution of the governing equations.

Numerical Treatment of Multiphase Flows in Porous Media, Lecture Notes in Physics, Vol. 552
Chen, Ewing, and Shi (eds.), pp. 35–49.

ISBN 3-540-67566-3

In its simplest form, one replaces the coefficients of the governing equations with an effective or macroscopic coefficient [5]. This works well in certain situations [9, 1], but not so well in others. Often it is necessary to change the form of the governing equations to obtain a suitable coarse-scale model [3]; there is no *a priori* reason to expect otherwise. Such is especially the case when nonlinearities are present, since it is well known that a function of an average is *not* the average of the function. Various techniques are used in this case, including homogenization [1, 10], the definition of pseudo-functions (altered forms of the nonlinear functions that appear in the governing equations), the use of renormalization methods [8], and many other techniques.

In terms of the simulation of flow and transport in a porous medium, our goal for nonlinear upscaling in this paper will be to resolve some of the finer scales in the solution directly, so that no loss of accuracy due solely to averaging will result. We will then be able to incorporate directly into the simulation relative and absolute permeability, porosity, capillary pressure, and well location information on scales smaller than the computational grid. That is, our nonlinear functions such as relative permeability and capillary pressure need not be modified, since the fine scales have been sufficiently resolved. Our technique is based on numerics. We assume that a fine grid fully represents the important physical scales, and that our computational grid is somewhat coarser. That is, perhaps some other homogenization technique has elevated the problem to a reasonable fine scale, but this fine scale is still too fine to compute over.

We present our ideas by considering first a problem representing incompressible, single-phase flow in a porous medium in the absence of gravity:

$$\begin{aligned} \nabla \cdot \mathbf{u} &= f, \\ \mathbf{u} &= -K\nabla p, \end{aligned} \tag{1}$$

where p is the pressure, K is the permeability divided by the fluid viscosity, $\mathbf{u}$ is the Darcy velocity, and f represents the wells. For simplicity, set $\mathbf{u} \cdot \nu = 0$ on the external boundary.

As an outline of the paper, we present in §2 a derivation of the upscaled equations for single phase flow, including a definition of our closure assumption. In §3 we give a mixed finite element approximation of the equations that is compatible with the closure assumption. A solution technique based on the computation of numerical Greens functions is given in §4. The accuracy of the method is discussed in §5. Finally in §6, we present briefly the two-phase problem, followed in §7 by some numerical results.

2 Derivation of the Upscaled Equations

We rewrite (1) in variational form as: Find $p \in W = L^2$ and $\mathbf{u} \in \mathbf{V} = H(\mathrm{div})$ such that

$$\begin{aligned} &\int \nabla \cdot \mathbf{u}\, w\, dx = \int f\, w\, dx && \forall\, w \in W, \\ &\int K^{-1}\, \mathbf{u} \cdot \mathbf{v}\, dx = -\int \nabla p \cdot \mathbf{v}\, dx = \int p\, \nabla \cdot \mathbf{v}\, dx && \forall\, v \in \mathbf{V}, \end{aligned} \tag{2}$$

where $H(\mathrm{div}) = \{\mathbf{v} \in (L^2)^3 : \nabla \cdot \mathbf{v} \in L^2, \mathbf{v} \cdot \nu = 0 \text{ on the external boundary}\}$.

Let W_c and $\mathbf{V}_c$ be the computationally resolvable parts of W and $\mathbf{V}$, and δW and $\delta \mathbf{V}$ the remainders. That is,

$$\begin{aligned} &W = W_c \oplus \delta W, && \mathbf{V} = \mathbf{V}_c \oplus \delta \mathbf{V}, \\ &p = p_c + \delta p \in W_c \oplus \delta W, && \mathbf{u} = \mathbf{u}_c + \delta \mathbf{u} \in \mathbf{V}_c \oplus \delta \mathbf{V}. \end{aligned}$$

2.1 Separation of scales

Separate the fine and δ-scales by restricting to appropriate test functions in the variational formulation. For the coarse scale, we have

$$\begin{aligned} &\int \nabla \cdot (\mathbf{u}_c + \delta \mathbf{u})\, w_c\, dx = \int f\, w_c\, dx && \forall\, w_c \in W_c, \\ &\int K^{-1}\, (\mathbf{u}_c + \delta \mathbf{u}) \cdot \mathbf{v}_c\, dx = \int (p_c + \delta p)\, \nabla \cdot \mathbf{v}_c\, dx && \forall\, \mathbf{v}_c \in \mathbf{V}_c, \end{aligned} \tag{3}$$

and for the δ-scale,

$$\begin{aligned} &\int \nabla \cdot (\mathbf{u}_c + \delta \mathbf{u})\, \delta w\, dx = \int f\, \delta w\, dx && \forall\, \delta w \in \delta W, \\ &\int K^{-1}\, (\mathbf{u}_c + \delta \mathbf{u}) \cdot \delta \mathbf{v}\, dx = \int (p_c + \delta p)\, \nabla \cdot \delta \mathbf{v}\, dx && \forall\, \delta \mathbf{v} \in \delta \mathbf{V}. \end{aligned} \tag{4}$$

If we were to ignore the δ-scales (i.e., perform no upscaling), then we would simply set $\delta \mathbf{u} = 0$, $\delta p = 0$, and use only the coarse equation (3). Upscaling concerns the treatment of these other terms and (4).

Given $(\mathbf{u}_c, p_c, f)$, we can solve for

$$\delta \mathbf{u} = \Phi_u(\mathbf{u}_c, p_c, f) \qquad \text{and} \qquad \delta p = \Phi_p(\mathbf{u}_c, p_c, f), \tag{5}$$

where Φ is a multi-linear operator. Thus (3) becomes

$$\begin{aligned} &\int \nabla \cdot (\mathbf{u}_c + \Phi_u(\mathbf{u}_c, p_c, f))\, w_c\, dx = \int f\, w_c\, dx && \forall\, w_c \in W_c, \\ &\int K^{-1}\, (\mathbf{u}_c + \Phi_u(\mathbf{u}_c, p_c, f)) \cdot \mathbf{v}_c\, dx \\ &\qquad = \int (p_c + \Phi_p(\mathbf{u}_c, p_c, f))\, \nabla \cdot \mathbf{v}_c\, dx && \forall\, \mathbf{v}_c \in \mathbf{V}_c, \end{aligned} \tag{6}$$

posed only on the coarse scale. We remark that no approximation has been made yet; all scales are fully resolved by (4)–(6). However, these two equations are intrinsically coupled, since Φ is a nonlocal operator.

2.2 Closure assumption (localization approximation)

Define a coarse computational grid and assume that

$$\delta\mathbf{V}\cdot\nu = 0 \qquad \text{on } \partial E_c \tag{7}$$

for each coarse element E_c. Then Φ (i.e., (4)) becomes a local operator:

$$\begin{aligned} &\textstyle\int_{E_c} \nabla\cdot(\mathbf{u}_c+\delta\mathbf{u})\,\delta w\,dx = \int_{E_c} f\,\delta w\,dx && \forall\,\delta w\in\delta W|_{E_c},\\ &\textstyle\int_{E_c} K^{-1}(\mathbf{u}_c+\delta\mathbf{u})\cdot\delta\mathbf{v}\,dx = \int_{E_c}(p_c+\delta p)\nabla\cdot\delta\mathbf{v}\,dx && \forall\,\delta\mathbf{v}\in\delta\mathbf{V}|_{E_c}. \end{aligned} \tag{8}$$

Condition (7) is our closure assumption. We have assumed that all net flux between coarse elements occurs only on the coarse scale.

3 Mixed Finite Element Approximation

We assume that nested fine and coarse computational grids are used, and let h and H be the grid spacings, respectively. The fine grid is assumed to be essentially what is needed to fully resolve the physical scales. Generally speaking, we envision H/h as a moderate integer (4 to 10, say).

We approximate (5)–(8) by a mixed finite element method. Other discretizations could be employed; however, the local conservation of these methods make them attractive for porous media simulation [12]. They approximate both the pressure and Darcy velocity directly.

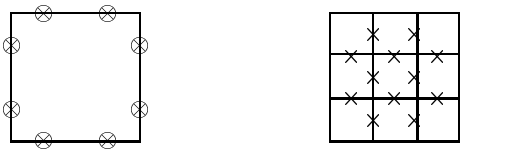

Coarse BDDF_1 velocities δ-scale RT_0 velocities

FIG. 1. The degrees of freedom of the approximating spaces.

As depicted in Fig. 1, we approximate the coarse equation (6) on the coarse grid with BDDF_1 spaces (BDM_1 in 2-D) [6, 7]. These spaces have 1 degree of freedom per coarse element for the pressure approximation, W_c, and 3 degrees of freedom per coarse element face (2 per edge in 2-D) for the velocity, $\mathbf{V}_c$. They are second order accurate in H for the velocity and first order for the pressure. The fine grid is used for the δ-equation (8). We use within each coarse element RT_0 spaces [11]. These have one degree

of freedom per fine element for the pressure approximation, δW, subject to the requirement of orthogonality to W_c that the average over the coarse element vanishes, and RT_0 has one degree of freedom per fine element face for the velocity, $\delta\mathbf{V}$, subject to the closure assumption (7). They are first order accurate in h for both the pressure and velocity for pressures with zero average over coarse elements and velocities with zero normal components on coarse element boundaries.

We remark that pressure is resolved fully on the fine scale, and formally approximated to first order in h. The fact that the BDDF_1 space approximates velocity to second order compensates for the closure assumption, which assumes all net flow between coarse elements is on the coarse scale. Without this choice, the results degrade significantly [4].

4 Solution by Numerical Greens Functions

We present now a technique to solve the system of equations efficiently. Before we elaborate, the outline of the technique is as follows.

1. Pre-solve for the influence of the coarse scale on the δ-scale. These are small disjoint problems, one for each coarse element, by (7). These pre-solutions are numerical Greens functions for the δ-problems (8).
2. Solve the coarse scale problem (6), accounting for the pre-solution response of the δ-scale to the coarse scale in (5).
3. Post-solve to combine results to form the fine-scale solution.

Integrals over coarse elements of the form $W_c * \delta W$ vanish by orthogonality. Since $\nabla\cdot\mathbf{V}_c = W_c$ and $\nabla\cdot\delta\mathbf{V} = \delta W$, integrals of $\nabla\cdot\delta\mathbf{V} * W_c$ and $\nabla\cdot\mathbf{V}_c * \delta W$ also vanish; thus, several terms in the equations below vanish.

4.1 Pre-solution

Locally on each coarse element E_c, let $\mathbf{v}_{c,i} \in \mathbf{V}_c$ have flux only at a single degree of freedom ($i = 1, ..., 18$ in 3-D and $i = 1, ..., 8$ in 2-D). Then

$$\mathbf{u}_c = \sum_i \alpha_i \mathbf{v}_{c,i}. \tag{9}$$

Solve the following problems for the numerical Greens functions.
Nonhomogeneous terms. Find $\delta\mathbf{u}_0 \in \delta\mathbf{V}$ and $\delta p_0 \in \delta W$ such that

$$\begin{aligned} \int \nabla\cdot\delta\mathbf{u}_0\,\delta w\,dx &= \int f\,\delta w\,dx \qquad && \forall\,\delta w \in \delta W|_{E_c}, \\ \int K^{-1}\delta\mathbf{u}_0\cdot\delta\mathbf{v}\,dx &= \int \delta p_0\,\nabla\cdot\delta\mathbf{v}\,dx \qquad && \forall\,\delta\mathbf{v} \in \delta\mathbf{V}|_{E_c}. \end{aligned} \tag{10}$$

Influence of $\mathbf{v}_{c,i}$. For each i, find $\delta\mathbf{u}_i \in \delta\mathbf{V}$ and $\delta p_i \in \delta W$ such that

$$\begin{aligned} &\int \nabla\cdot\delta\mathbf{u}_i\,\delta w\,dx = 0 && \forall\,\delta w \in \delta W|_{E_c},\\ &\int K^{-1}(\mathbf{v}_{c,i}+\delta\mathbf{u}_i)\cdot\delta\mathbf{v}\,dx = \int \delta p_i\,\nabla\cdot\delta\mathbf{v}\,dx && \forall\,\delta\mathbf{v} \in \delta\mathbf{V}|_{E_c}. \end{aligned} \tag{11}$$

Note that the combinations

$$\begin{aligned} &\delta\mathbf{u}_0 + \textstyle\sum_i \alpha_i\,\delta\mathbf{u}_i \equiv \Phi_u(\mathbf{u}_c, f) = \delta\mathbf{u},\\ &\delta p_0 + \textstyle\sum_i \alpha_i\,\delta p_i \equiv \Phi_p(\mathbf{u}_c, f) = \delta p \end{aligned} \tag{12}$$

depend linearly on the (as yet unknown) nodal values of $\mathbf{u}_c$ and on the numerical Greens functions and give $\delta\mathbf{u}$ and δp solving (8).

4.2 Coarse Solution

Given the numerical Greens functions and the implicit representation of the upscaling operator (12), we can now reformulate (6) as a problem for the course unknowns only. We find $\mathbf{u}_c \in \mathbf{V}_c$ and $p_c \in W_c$ such that

$$\begin{aligned} &\int \nabla\cdot\mathbf{u}_c\,w_c\,dx = \int f\,w_c\,dx && \forall\,w_c \in W_c,\\ &\int K^{-1}(\mathbf{u}_c+\Phi_u(\mathbf{u}_c,f))\cdot\mathbf{v}_c\,dx = \int p_c\,\nabla\cdot\mathbf{v}_c\,dx && \forall\,\mathbf{v}_c \in \mathbf{V}_c. \end{aligned} \tag{13}$$

We rewrite this system with $\mathbf{v}_c = \mathbf{v}_j$ using that

$$\begin{aligned} &\mathbf{u} = \mathbf{u}_c + \delta\mathbf{u} = \delta\mathbf{u}_0 + \textstyle\sum_i \alpha_i\,(\mathbf{v}_{c,i}+\delta\mathbf{u}_i),\\ &p = p_c + \delta p = p_c + \delta p_0 + \textstyle\sum_i \alpha_i\,\delta p_i, \end{aligned} \tag{14}$$

and using (10)–(11) with $\delta\mathbf{v} = \delta\mathbf{u}_j$ and orthogonality as

$$\begin{aligned} &\textstyle\sum_i \alpha_i \int \nabla\cdot(\mathbf{v}_{c,i}+\delta\mathbf{u}_i)\,w_c\,dx = \int f\,w_c\,dx,\\ &\textstyle\sum_i \alpha_i \int K^{-1}(\mathbf{v}_{c,i}+\delta\mathbf{u}_i)\cdot(\mathbf{v}_{c,j}+\delta\mathbf{u}_j)\,dx\\ &\qquad = \textstyle\int (p_c+\delta p_0)\,\nabla\cdot(\mathbf{v}_{c,j}+\delta\mathbf{u}_j)\,dx - \int K^{-1}\delta\mathbf{u}_0\cdot(\mathbf{v}_{c,j}+\delta\mathbf{u}_j)\,dx. \end{aligned} \tag{15}$$

Thus the method is similar to an "optimal test function" method where we replace $\mathbf{v}_c$ by $\mathbf{v}_{c,j}+\delta\mathbf{u}_j$; however, we also add some nonhomogeneous terms that improve the accuracy over such "optimal" methods.

4.3 Post-solution

Given $\mathbf{u}_c$, p_c, and the numerical Greens functions, compute (14) on the fine scale to obtain a "fully resolved" approximation of the true solution.

5 Accuracy

Denote by $\|\cdot\|$ the L^2-norm, and by P_{W_c}, P_{W_f}, and $P_{\delta W}$ the L^2-projections into W_c, the full fine grid space $W_f = W_c \oplus \delta W$, and δW, respectively.

If we solve the entire problem (2) for $(\mathbf{u}_f, p_f) \in \mathrm{RT}_0$ over the entire fine mesh or for $(\mathbf{u}_c, p_c) \in \mathrm{BDDF}_1$ (or BDM_1 in 2-D) on the coarse mesh, we see the following error estimates [11, 6, 7], where $(\mathbf{u}, p)$ is the true solution.

Theorem 5.1 *For RT_0 with no upscaling on the fine mesh, for $\mathbf{v} \in \mathbf{V}_f$ such that $\nabla \cdot \mathbf{v} = P_{W_f} f$,*

$$\|K^{-1/2}(\mathbf{u} - \mathbf{u}_f)\| \leq \inf_{\mathbf{v}} \|K^{-1/2}(\mathbf{u} - \mathbf{v})\| \leq Ch,$$
$$\|p - p_f\| \leq Ch.$$

For $BDDF_1$ (or BDM_1) with no upscaling on the coarse mesh, for $\mathbf{v} \in \mathbf{V}_c$ such that $\nabla \cdot \mathbf{v} = P_{W_c} f$,

$$\|K^{-1/2}(\mathbf{u} - \mathbf{u}_c)\| \leq \inf_{\mathbf{v}} \|K^{-1/2}(\mathbf{u} - \mathbf{v})\| \leq CH^2,$$
$$\|p - p_c\| \leq CH.$$

The upscaling technique displays elements of both estimates above. It is easy to prove the following error estimate.

Theorem 5.2 *For $BDDF_1$ (or BDM_1) upscaled with the RT_0 subgrid approximation, for $\mathbf{v} \in \mathbf{V}_c + \delta\mathbf{V}$ such that $\nabla \cdot \mathbf{v} = P_{W_f} f$, $\mathbf{v}_c \in \mathbf{V}_c$ such that $\nabla \cdot \mathbf{v}_c = P_{W_c} f$, and $\delta\mathbf{v} \in \delta\mathbf{V}$ such that $\nabla \cdot \delta\mathbf{v} = P_{\delta W} f$,*

$$\begin{aligned}\|K^{-1/2}(\mathbf{u} - (\mathbf{u}_c + \delta\mathbf{u}))\| &\leq \inf_{\mathbf{v}} \|K^{-1/2}(\mathbf{u} - \mathbf{v})\| \\ &\leq \inf_{\bar{\mathbf{u}}, \mathbf{v}_c, \delta\mathbf{v}} \left\{ \|K^{-1/2}(\bar{\mathbf{u}} - \mathbf{v}_c)\| + \|K^{-1/2}(\mathbf{u} - \bar{\mathbf{u}} - \delta\mathbf{v})\| \right\}, \\ \|p - p_c\| &\leq CH.\end{aligned}$$

While it is difficult to interpret the velocity error, we should expect better bounds than in Theorem 5.1; that is, we should expect the velocity error to be second order. Our numerical results suggest that this is indeed the case, and that the error has in fact no simple form (as indicated in the theorem). We consider two test cases in which $K = 1$ on a unit square domain and we use Dirichlet boundary conditions and f defined from the imposed true solution $p(x, y) = xy^3 + x^2 y \cos(xy)$ or $1/(1 + \exp(10x + 10y^2 - 3y - 5))$, respectively.

It is readily apparent from the data in Table 1, that if H/h is fixed, the error in pressure is $O(H) = O(h)$, and the error in velocity is $O(H^2) = O(h^2)$, as we would expect. However, if H/h is *not* fixed, the results are much less predictable. For the tests reported and a few more conducted, the best fit of the L^2-error in $\mathbf{u}$ is $E_u^1 = 150H^2 + 360H^{1/2}h^{3/2}$ and $E_u^2 = 1000H^2 + 8000H^{1/4}h^{7/4}$, respectively for the two cases, and for the pressure

p, the error is $E_p^1 = 0.36h + 0.0003H$ and $E_p^2 = 0.4h + 0.0006H^{1.7}h^{-0.7}$, respectively. Thus the error depends in a complicated way on the solution and probably on H/h, but p is first order and $\mathbf{u}$ is second order accurate.

It is interesting to note from Table 1 that the error in the pressure is dominated by the fine mesh size, nearly independently of the coarse mesh.

Case 1				Case 2			
$1/h$	$1/H$	Pressure	Velocity	$1/h$	$1/H$	Pressure	Velocity
10	10	0.0359	5.63	10	10	0.0438	173.64
20	20	0.0180	1.42	20	20	0.0219	47.08
40	40	0.0090	0.36	40	40	0.0109	12.03
80	80	0.0045	0.16	80	80	0.0055	3.03
10	2	0.0359	46.79	10	2	0.0440	413.35
20	4	0.0180	11.14	20	4	0.0220	185.70
40	8	0.0090	2.76	40	8	0.0109	43.25
80	16	0.0045	0.69	80	16	0.0055	10.82
160	4	0.0023	8.97	80	2	0.0095	273.92
160	8	0.0022	2.26	80	4	0.0060	159.92
160	16	0.0022	0.60	80	8	0.0055	36.50
160	32	0.0022	0.18	80	16	0.0055	10.82
10	2	0.0359	46.79	10	2	0.0440	413.35
20	2	0.0180	41.09	20	2	0.0230	310.56
40	2	0.0091	39.39	40	2	0.0134	281.47
80	2	0.0046	38.94	80	2	0.0095	273.92

Table 1. Some L^2-errors for Cases 1 and 2.

6 Two-phase Immiscible, Incompressible Flow

We now turn to a nonlinear problem describing the flow of two immiscible, incompressible fluids in a porous medium, such as oil and water. For phase $j = w, o$ (i.e., water and oil), let s_j, $\mathbf{u}_j$, and p_j be the phase saturations, Darcy velocities, and pressures. Let $s = s_w = 1 - s_o$, ϕ be the porosity, K the absolute permeability, g the gravitational constant, and z the depth. The mobilities are related to the relative permeabilities and fluid viscosities as $\lambda_j(s) = k_{r,j}(s)/\mu_j$ and $\lambda(s) = \lambda_w(s) + \lambda_o(s)$, and $P_c(s) = p_o - p_w$ is the capillary pressure. Conservation of mass of each phase gives the governing equations. After reformulation, we obtain the following (see, e.g., [2]).

Pressure equation:

$$\begin{aligned} \nabla \cdot \mathbf{u} &= f \equiv f_w + f_o, \\ \mathbf{u} &= -K\lambda(s)(\nabla p - \rho(s)\nabla z), \end{aligned} \tag{16}$$

where the global pressure and density are

$$p = p_o - \int_0^s \frac{\lambda_w(\sigma)}{\lambda(\sigma)} P_c'(\sigma)\, d\sigma \qquad \text{and} \qquad \rho(s) = \frac{\lambda_w(s)}{\lambda(s)}\rho_w + \frac{\lambda_o(s)}{\lambda(s)}\rho_o.$$

Saturation equation:

$$\begin{aligned} &\phi \tfrac{\partial s}{\partial t} + \nabla \cdot \mathbf{u}_w = f_w(s), \\ &\mathbf{u}_w = -K\nabla q(s) + \gamma(\mathbf{u}, s), \end{aligned} \tag{17}$$

where the "complementary" potential and γ are

$$\begin{aligned} q(s) &= -\textstyle\int_0^s \frac{\lambda_w(\sigma)\lambda_o(\sigma)}{\lambda(\sigma)}\, P_c'(\sigma)\, d\sigma, \\ \gamma(\mathbf{u}, s) &= \tfrac{\lambda_w(s)}{\lambda(s)}\mathbf{u} - K\tfrac{\lambda_w(s)\lambda_o(s)}{\lambda(s)}(\rho_o - \rho_w) g \nabla z. \end{aligned}$$

We use sequential time splitting, a backward Euler time discretization, and integration-by-parts (3 times) to obtain the following variational form and time approximation for $\Delta t > 0$ and time levels $t^n = n\Delta t$.

Pressure equation:

$$\begin{aligned} &\textstyle\int \nabla \cdot \mathbf{u}^n\, w\, dx = \int f^n\, w\, dx, \\ &\textstyle\int (\lambda(s^{n-1})K)^{-1}\mathbf{u}^n \cdot \mathbf{v}\, dx = \int p^n\, \nabla \cdot \mathbf{v}\, dx + \int \rho(s^{n-1})\nabla z \cdot \mathbf{v}\, dx. \end{aligned} \tag{18}$$

Saturation equation: (wherein $w \in W_f = W_c \oplus \delta W$)

$$\begin{aligned} &\textstyle\int_{E_f} \phi \frac{s^n - s^{n-1}}{\Delta t}\, w\, dx + \int_{E_f} \nabla \cdot \psi^n\, w\, dx + \int_{\partial E_f} \gamma(\mathbf{u}^n, s^n_{\text{up}}) \cdot \nu\, w\, ds \\ &\qquad = \textstyle\int_{E_f} f_w^n(s^n)\, w\, dx, \\ &\textstyle\int K^{-1}\psi^n \cdot \mathbf{v}\, dx = \int q(s^n)\, \nabla \cdot \mathbf{v}\, dx, \end{aligned} \tag{19}$$

where $\psi^n = -K\nabla q(s^n)$, $\mathbf{u}_w^n = \psi^n + \gamma(\mathbf{u}^n, s^n)$, and we use one-point upstream weighting on the term involving γ.

As in the single-phase case, we separate the solution into coarse and fine scales $\mathbf{V}_c \oplus \delta\mathbf{V}$ or $W_c \oplus \delta W$:

$$\begin{aligned} \mathbf{v} = \mathbf{v}_c + \delta\mathbf{v}, \qquad \mathbf{u} = \mathbf{u}_c + \delta\mathbf{u}, \qquad \psi = \psi_c + \delta\psi, \\ w = w_c + \delta w, \qquad p = p_c + \delta p. \end{aligned} \tag{20}$$

Because the saturation equation is parabolic, it turns out that we do *not* need to decompose $s \in W_f$.

The pressure equation is linear and independent of the saturation equation, given s^{n-1}. We can solve for the upscaled $\mathbf{u}^n$ and p^n as above.

We linearize the saturation equation with Newton-Raphson, and solve for changes in s^n and ψ^n, given $\mathbf{u}^n$, using numerical Greens functions as in the linear case above. Upstream weighting on the fine scale destroys our localization assumption. To circumvent this, we simply use the old Newton result for the upstream value when it traces out of a coarse element.

7 Some numerical examples

We present two 2-D examples to illustrate our upscaling technique. In both, we have a square domain with uniform rectangular grids. The initial water saturation is 0.2. An injection well is placed in the lower left corner injecting water at a rate of $0.2\,\mathrm{m}^2/\mathrm{day}$, and a production well is in the adjacent corner. Time steps vary from 1 day initially to 25 days near the end of the simulations. The porosity is 0.25, but the permeability is heterogeneous.

7.1 Example 1

In this example, we have a 40 meter by 40 meter domain with a 40×40 fine grid. The base 10 logarithm of the permeability field is shown in Fig. 2.

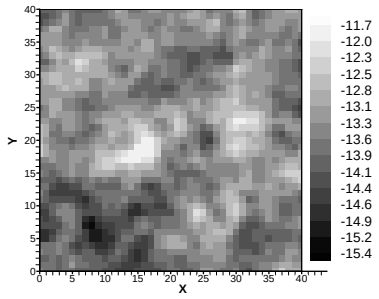

FIG. 2. The log of the permeability field for Example 1.

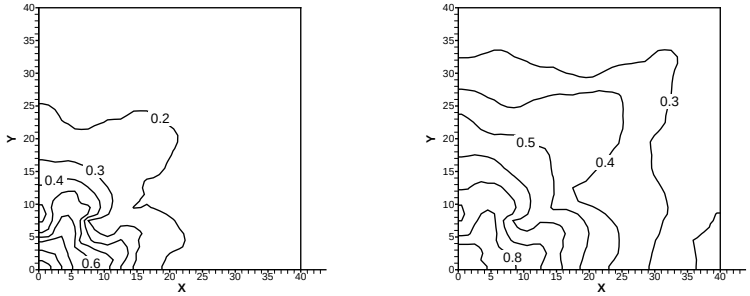

FIG. 3. Fine-scale saturation at 100 and 500 days for Example 1.

As can be seen in Figs. 3–4, the upscaling procedure approximates the saturation quite well. Here we use a 5×5 coarse grid, so on each coarse block, we have an 8×8 subgrid for the δ-problems. The coarse solution (Fig. 5) completely fails to resolve the flow and location of the wells.

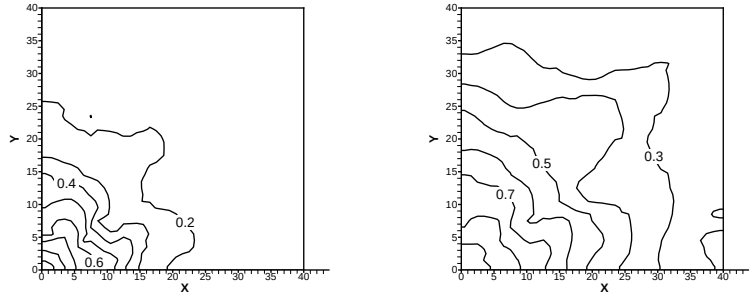

FIG. 4. 5×5 Upscaled saturation at 100 and 500 days for Example 1.

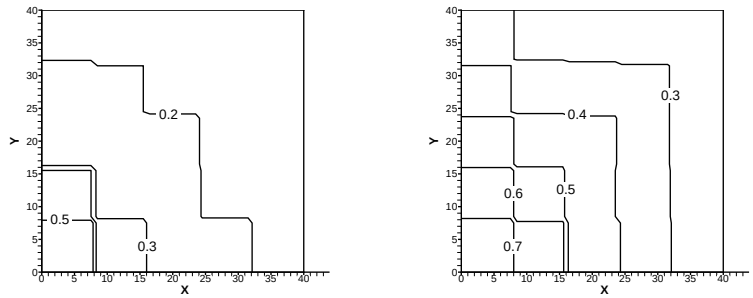

FIG. 5. Coarse-scale saturation at 100 and 500 days for Example 1.

In Figs. 6–7, we show the results of upscaling with 2×2 and 8×8 coarse grids (20×20 and 5×5 subgrids). Both perform quite well. The coarsest example does a very good job near the well, but the performance degrades later in time a bit as the flow reaches the middle of the domain.

The number of degrees of freedom used in these examples is given in Table 2. The coarse solution is woefully inadequate; however, for the cost of a global problem of the same size, we can upscale to a very reasonable level of resolution.

	Coarse grid		
	2×2	5×5	8×8
Coarse Velocity	8	80	224
Upscale Velocity	3048	2880	2784
Fine Velocity	6240	6240	6240
Coarse Pressure	4	25	64
Upscale Pressure	1600	1600	1600
Fine Pressure	1600	1600	1600

Table 2. Number of degrees of freedom for Example 1.

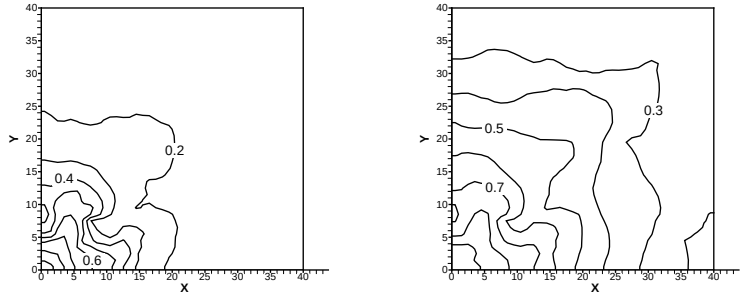

FIG. 6. 2×2 Upscaled saturation at 100 and 500 days for Example 1.

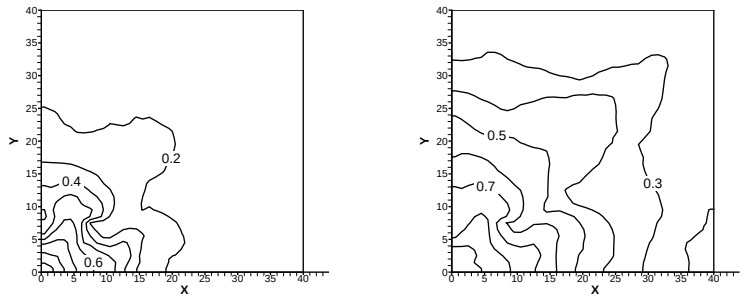

FIG. 7. 8×8 Upscaled saturation at 100 and 500 days for Example 1.

7.2 Example 2

In the second example, we have a 24×24 meter domain with a 24×24 fine grid and a 4×4 coarse grid. The base 10 logarithm of the permeability is depicted in Fig. 8. It has two high permeability streaks, akin to fractures.

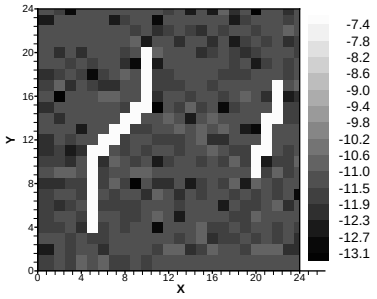

FIG. 8. The log of the permeability field for Example 2.

Fig. 9 shows that the saturation is very difficult to resolve. The upscaling technique does a reasonable job following the flow into the first high permeability streak. The coarse solution in Fig 10, however, completely misses the high permeability streaks. It shows an overall tendency to flow right to left rather than the proper direction down to up. The number of degrees of freedom used in this example is given in Table 3.

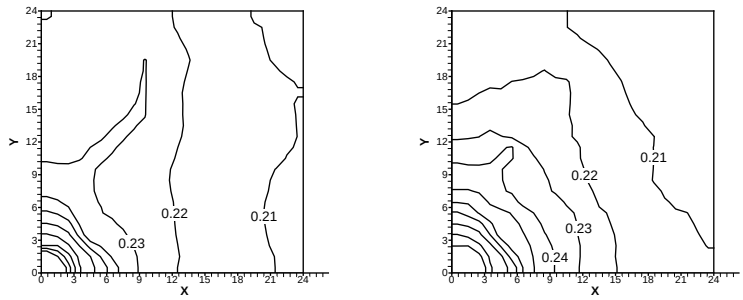

FIG. 9. Fine-scale and 4×4 Upscaled saturation at 20 days for Example 2.

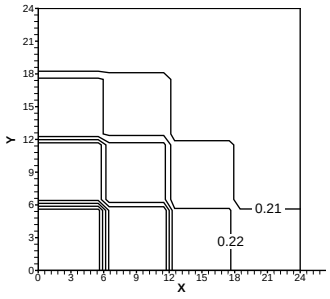

FIG. 10. Coarse-scale saturation at 20 days for Example 2.

	Velocity	Pressure
Coarse	48	16
Upscale	1008	576
Fine	2208	576

Table 3. Number of degrees of freedom for Example 2.

Some timing results are given in Table 4. The pressure equation is solved with Jacobi preconditioned conjugate gradients, the saturation equation by Jacobi preconditioned orthomin, and the upscaling numerical Greens functions by a direct solver. The time to compute the 24×24 fine scale solution

is quite high, since the problem is very poorly conditioned. In contrast, the 4×4 coarse problem is solved easily. In this example, the upscaled problem takes about as long to solve as the coarse problem; computing the numerical Greens functions takes little extra time and gives a much improved solution.

Steps	Fine	Upscale	Coarse
1	2:03	0:10	0:08
2	1:48	0:09	0:08
3–10	11:32	1:10	1:05
11–20	13:29	1:28	1:21
21–36		2:21	2:13
37–48	35:47	2:02	1:52
49–58		1:42	1:33
59–65	30:26	1:21	1:14
66–72		1:21	1:14
73–76	19:22	0:46	0:42
77–84	38:48	1:34	1:25

Table 4. Some timing results for Example 2.

8 Conclusions

Our upscaling approach improves the resolution of the computed solution. It allows recovery of fine-scale pressure, velocity, and saturation, so it incorporates fine-scale information and nonlinearities directly, thereby circumventing the need to define pseudo-functions. The technique resolves positions of wells within grid blocks, is efficient to compute, has good convergence properties, can be applied at each time step of a time dependent problem, and can be applied to a nonlinear problem during a Newton linearization step.

Acknowledgments. This work was supported by the U.S. National Science Foundation under grants DMS-9707015 and SBR-9873326.

References

[1] B. Amaziane, A. Bourgeat, and J. Koebbe, Numerical simulation and homogenization of two-phase flow in heterogeneous porous media, *Transport in Porous Media*, **9** (1991), 519–547.

[2] T. Arbogast, The existence of weak solutions to single-porosity and simple dual-porosity models of two-phase incompressible flow, *J. Nonlinear Analysis: Theory, Methods, and Applic.*, **19** (1992), 1009–1031.

[3] T. Arbogast, Gravitational forces in dual-porosity systems. I. Model derivation by homogenization and II. Computational validation of the homogenized model, *Transport in Porous Media*, **13** (1993), 179–220.

[4] T. Arbogast, S. E. Minkoff, and P. T. Keenan, An operator-based approach to upscaling the pressure equation, in *Computational Methods in Water Resources XII*, v. 1, V. N. Burganos et al., eds., Computational Mechanics Publications, Southampton, U.K., 1998, 405–412.

[5] A. Bensoussan, J. L. Lions, and G. Papanicolaou, *Asymptotic Analysis for Periodic Structure*, North Holland, Amsterdam, 1978.

[6] F. Brezzi, J. Douglas, Jr., R. Duràn, and M. Fortin, Mixed finite elements for second order elliptic problems in three variables, *Numer. Math.*, **51** (1987), 237–250.

[7] F. Brezzi, J. Douglas, Jr., and L. D. Marini, Two families of mixed elements for second order elliptic problems, *Numer. Math.*, **88** (1985), 217–235.

[8] M. A. Christie, M. Mansfield, P. R. King, J. W. Barker, and I. D. Culverwell, A renormalization-based upscaling technique for WAG floods in heterogeneous reservoirs, SPE 29127, in *Thirteenth Symp. on Reservoir Simulation*, Society of Petroleum Engineers, Feb. 1995, 353–361.

[9] L. J. Durlofsky, Numerical calculation of equivalent grid block permeability tensors for heterogeneous porous media, *Water Resources Research*, **27** (1991), pp. 699–708.

[10] T. Y. Hou and X. H. Wu, A multiscale finite element method for elliptic problems in composite materials and porous media, *J. Comput. Phys.*, **134** (1997), 169–189.

[11] R. A. Raviart and J. M. Thomas, A mixed finite element method for 2nd order elliptic problems, in *Mathematical Aspects of the Finite Element Method*, Springer-Verlag, New York, 1977, 292–315.

[12] T. F. Russell and M. F. Wheeler, Finite element and finite difference methods for continuous flows in porous media, in *The Mathematics of Reservoir Simulation*, R. E. Ewing, ed., Society for Industrial and Applied Mathematics, Philadelphia, 1983, Chapter II.

Todd Arbogast
Department of Mathematics; C1200
The University of Texas at Austin
Austin, TX 78712 USA
arbogast@math.utexas.edu